Quaternized Silicon Nanoparticles with Polarity-Sensitive Fluorescence for Selectively Imaging and Killing Gram-Positive Bacteria

Xiaodong Zhang, Xiaokai Chen, Jingjing Yang, Hao-Ran Jia, Yan-Hong Li, Zhan Chen,* and Fu-Gen Wu*

X. D. Zhang, X. K. Chen, J. J. Yang, H. R. Jia, Y. H. Li, Prof. F. G. Wu

State Key Laboratory of Bioelectronics, School of Biological Science and Medical Engineering,

Southeast University, Nanjing 210096, P. R. China

E-mail: wufg@seu.edu.cn

Prof. Z. Chen

Department of Chemistry, University of Michigan, 930 North University Avenue, Ann Arbor,

Michigan 48109, United States

E-mail: zhanc@umich.edu

Author Manuscript

Abstract

With the emergence of antibiotic resistance, developing new antibiotics and therapies for combating bacterial infections is urgently needed. Herein, a series of quaternized fluorescent silicon nanoparticles (SiNPs) were facilely prepared by the covalent reaction between amine-functionalized SiNPs and carboxyl-containing *N*-alkyl betaines. It was found that the bactericidal efficacy of these quaternized SiNPs increased with the length of the *N*-alkyl chain, and SiNPs conjugated with *N*,*N*-dimethyl-*N*-octadecylbetaine (BS-18), abbreviated as SiNPs-C$_{18}$, showed the best antibacterial effect, whose minimum inhibitory concentrations (MICs) for Gram-positive bacteria were 1.0–2.0 μg/mL. In vivo tests further confirmed that SiNPs-C$_{18}$ had excellent antibacterial efficacy and greatly reduced bacterial load in the infectious sites. The SiNPs-C$_{18}$ exhibited low cytotoxicity towards mammalian cells (including normal liver and lung cells, red blood cells, and macrophages), enabling them to be useful for clinical applications. Besides, the quaternized SiNPs exhibited polarity-dependent fluorescence emission property and could selectively image Gram-positive bacteria, thereby providing a simple method to successfully differentiate Gram-positive and Gram-negative bacteria. The present work represents the first example that successfully turns fluorescent SiNPs into metal-free NP-based antibiotics with simultaneous bacterial imaging and killing capability, which broadens the applications of fluorescent SiNPs and advances the development of novel antibacterial agents.

1. Introduction

Bacteria can cause life-threatening human diseases and afflict millions of people annually.[1] The most widely used methods to treat bacterial infection are therapies with antibiotics. However, traditional antibiotics are becoming less efficient because of the development of drug-resistant bacterial strains.[2] To deal with microbial drug resistance, nanoparticle (NP)-based antibiotics have been extensively researched in the recent years. For instance, Jiang *et al.* discovered that AuPt bimetallic NPs could rupture the bacterial inner membrane and increase intracellular adenosine triphosphate (ATP) levels, with the minimal inhibitory concentration (MIC) of 5 µg/mL for *Escherichia coli* (*E. coli*).[3] Liu and Peng *et al.* developed a graphene oxide-based iron oxide and silver co-deposited nanocomposite as an effective, multifunctional, and recyclable antibacterial agent, with greatly enhanced antibacterial efficiency toward both Gram-negative bacteria *E. coli* and Gram-positive bacteria *Staphylococcus aureus* (*S. aureus*).[4] Recently, Rottelo *et al.* demonstrated the use of functionalized Au NPs to combat multi-drug-resistant pathogenic bacteria, and the bacterial resistance was not observed after even 20 generations.[5] He and Peng *et al.* reported silicon-containing antibacterial materials made of silver nanoparticle-decorated silicon wafers, which featured stable and high antibacterial activity, preserving >99% antibacterial efficiency against *E. coli* for 30 days.[6] Overall, NPs provide excellent platforms for antibacterial applications with many advantages due to their unique characteristics.[7] For example, the versatile size, shape, and chemical characteristics enable NPs to facilitate

molecular interactions with bacteria, optimizing their action in vitro and in vivo.[8] The high

surface to volume ratio allows incorporation of abundant functional ligands to NPs, enabling

multi-valency on NP surface to further enhance interactions with bacteria.[5] Furthermore,

NPs may passively target to and be accumulated in the bacterium-infected sites because

these sites have enhanced permeability and retention (EPR) effect for NPs.[9] Meanwhile,

NP-based drug delivery platforms, such as mesoporous NPs, have been increasingly

exploited for slow-released antimicrobial materials.[10]

Among many NPs reported as antibacterial agents, the most widely explored silver

(Ag)-containing NPs[11] and other metal-containing NPs[12] may have limitations in use due to

their cytotoxicity or possible long-term in vivo retention. Recently, metal-free NPs such as

graphene oxide,[13] polymer nanocomposites,[14] liposome,[15] and cationic peptide NPs[16]

have been developed, but there are few developments of the antibacterial agents based on

metal-free and fluorescent NPs, such as silicon NPs and carbon dots.

In addition to fighting against bacterial drug resistance, fast diagnosis is also important for

bacterial infection treatment. Gram staining method invented in 1884 is the standard

diagnostic method for characterizing unknown bacteria, classifying bacteria into

Gram-positive and Gram-negative ones. Some antibiotics such as penicillin are usually

effective against Gram-positive but not for Gram-negative bacteria. Others such as

streptomycin are the opposite. The Gram staining method has complicated procedures and

may easily generate false positive results, therefore other methods have also been developed to differentiate Gram-positive from Gram-negative ones. For example, Ryu reported a fast and general way using a solution of potassium hydroxide in 1938,[17] but this method is not applicable for a sample containing both Gram-positive and Gram-negative bacteria. Fluorescent wheat germ agglitinin (WGA) conjugates were used to image Gram-positive bacteria selectively by Sizemore *et al*.[18] However, a recent study demonstrated that some WGA conjugates could also stain Gram-negative bacteria.[19] Recently, vancomycin- and daptomycin-modified NPs have been synthesized to target the cell walls of Gram-positive bacteria,[20] but the use of these antibiotics for bacteria detection may lead to unexpected drug resistance. Besides, since vancomycin and daptomycin may target both Gram-positive bacteria and Gram-negative bacteria, the results may not be always accurate.

In the recent years photoluminescent silicon nanoparticles (SiNPs) have received much attention, which possess many superior characteristics including excellent optical properties, easy surface modification capability, and low cytotoxicity.[21] Owing to their hyperfluorescence and photostability, SiNPs should be an ideal fluorescent probe used for bacterial detection and imaging if they can selectively target bacteria. The size range of SiNPs is commensurate with biomolecules, enabling them to cross through blood vessels, penetrate tissues rapidly, and accumulate in the bacteria-infected sites. Although SiNPs have been extensively employed in a large variety of applications, including

6

optoelectronics,[22] energy,[23] catalysis,[24] and biology (bioanalysis, bioimaging, and anticancer drug delivery),[25] according to the best of our knowledge, the reports on the development of SiNPs as antibacterial and bacterial imaging agents are still lacking.

Previously we have used a simple method to prepare a series of fluorescent SiNPs with quantum efficiency even larger than 80%, which have a great potential in many applications related to bio-imaging.[25a,26] In this study, inspired by the excellent fluorescence property of SiNPs and the promising antibacterial effect of quaternary ammonium compounds, we prepared a series of surface modified SiNPs (we will use a simple name of "quaternized SiNPs" to represent such SiNPs below) using a simple reaction between the amine groups on the surface of SiNPs and the carboxyl groups of *N*-alkyl betaines (**Scheme 1**). We will organize our results reported in this article in the following way: the synthesis and characterization of quaternized SiNPs, the selective imaging and successful differentiation of Gram-positive and Gram-negative bacteria by the quaternized SiNPs, the in vitro and in vivo antibacterial activity and selectivity, and the safety evaluation of the quaternized SiNPs.
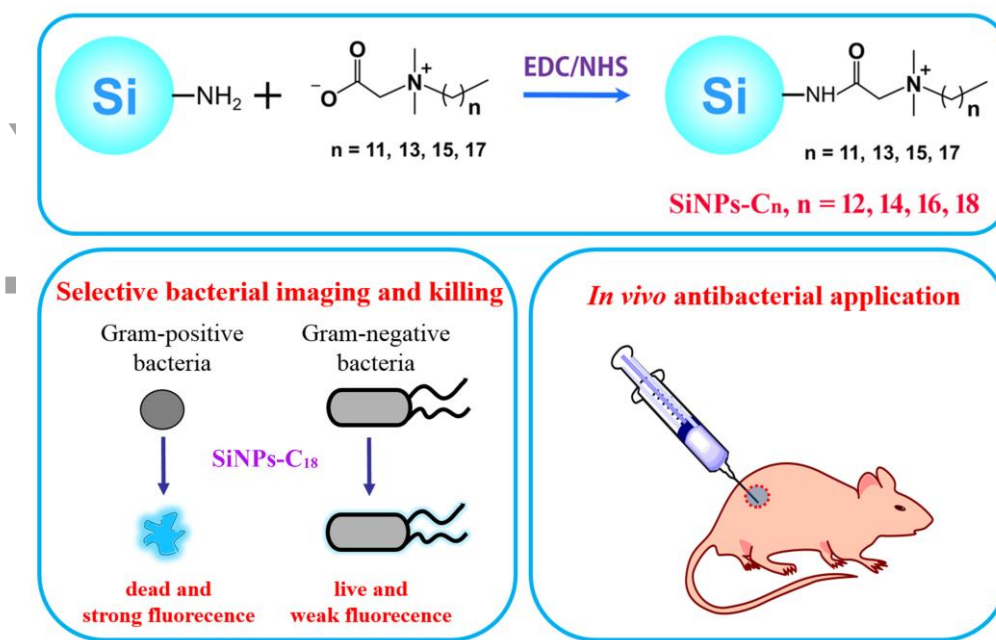
Scheme 1. Schematics of the synthetic route of quaternized SiNPs, the selective bacterial killing and imaging of quaternized SiNPs, and the corresponding in vivo antibacterial application.

2. Results and Discussion

2.1. Preparation and Characterization of Quaternized SiNPs

The amine-containing water-soluble SiNPs were prepared using (3-aminopropyl)trimethoxysilane (APTMS) and trisodium citrate by our previously reported microwave-assisted method,[25a,26] with an average diameter of ~2.4 nm. To prepare quaternized SiNPs, a series of *N*-alkyl betaines, including *N*,*N*-dimethyl-*N*-laurylbetaine (abbreviated as BS-12), *N*,*N*-dimethyl-*N*-myristylbetaine (abbreviated as BS-14),

N,*N*-dimethyl-*N*-hexadecylbetaine (abbreviated as BS-16), and

N,*N*-dimethyl-*N*-octadecylbetaine (abbreviated as BS-18), were conjugated to the SiNPs

using the reaction between the carboxyl groups of *N*-alkyl betaines and the amine groups of

SiNPs (Scheme 1). The SiNP products prepared with different *N*-alkyl betaines were named

as SiNPs-C_{12}, SiNPs-C_{14}, SiNPs-C_{16}, and SiNPs-C_{18}, respectively. The number 12, 14, 16, or 18

indicates the hydrocarbon chain length of the betaine molecule attached to the quaternary

ammonium nitrogen atom. The prepared quaternized SiNPs were characterized using a

variety of analytical techniques. The results of SiNPs-C_{18} are shown below as representative

examples. The TEM image (**Figure 1**a) showed that SiNPs-C_{18} had an average diameter of 2.8

nm, which is slightly larger than original SiNPs. A substantial increase of the SiNP surface

potential in phosphate buffered saline (PBS, pH = 7.2) from − 2.1 ± 0.5 to + 13.4 ± 1.6 mV

after conjugation with BS-18 was observed, indicating the successful coupling of the *N*-alkyl

betaine molecules to SiNPs. In FTIR spectra (Figure 1b), the similar absorbance peaks at

~1463−1472, 2850, and 2920 cm^{-1} (attributed to the CH_2 bending, symmetric CH_2 stretching,

and asymmetric CH_2 stretching, respectively) observed for both BS-18 and SiNPs-C_{18} came

from the CH_2 vibrations of the hydrocarbon chains of BS-18 molecules, showing that BS-18

molecules were successfully attached to the SiNPs. This is well correlated to the above

surface potential measurement result. The signal contributed by the Si−O−Si stretching

vibration at ~1120 cm^{-1} observed from both SiNPs and SiNPs-C_{18} suggested that the

prepared SiNPs-C_{18} still contained the Si−O−Si network. In addition, two new peaks at 1643

and 1578 cm^{-1}, attributed to the vibrations of the amide bonds formed between carboxyl and amine groups, were observed in SiNPs-C$_{18}$, which further proves the covalent linkage between BS-18 and SiNPs. Furthermore, XPS spectra (Figure 1c and d) were collected to determine the chemical compositions of SiNPs-C$_{18}$. As shown in Figure 1c, SiNPs-C$_{18}$ contain the C, N, and O elements in addition to Si. The high resolution spectrum of N 1s in SiNPs-C$_{18}$ (Figure 1d) exhibited two peaks at 398.8 and 402.8 eV, which can be attributed to C−N−C and quaternary-N, respectively. The XPS results further confirmed the composition of SiNPs-C$_{18}$, in good agreement with the above zeta potential and IR results. We also collected the UV–vis absorption spectra from the SiNPs, BS-18, and SiNPs-C$_{18}$ (Figure 1e). Free BS-18 exhibited no obvious peak, while the absorption peak of SiNPs shifted from 348 to 262 nm after conjugation with BS-18, which is similar with that of alkyl-functionalized SiNPs as previously reported.[27] All the evidence proved that *N*-alkyl betaine molecules were successfully conjugated to the SiNPs.

To investigate the stability of the product, SiNPs-C$_{18}$ were dissolved in different solutions including water, normal saline (0.9% NaCl), PBS, and lysogeny broth (LB) medium. Clear solutions were observed for all these samples and no precipitates were formed within six months (inset, Figure 1e), suggesting that SiNPs-C$_{18}$ have superior stability and should be suitable for antibacterial application.

Besides the stability, the fluorescence properties of SiNPs-C$_{18}$ were also studied. The maximum emission peak of SiNPs-C$_{18}$ was observed to be ~450 nm under the 348 nm excitation, which has a 6-nm red shift compared to that of SiNPs. Using quinine sulfate as a reference, the photoluminescence quantum yield (PLQY) was measured to be ~3.0%. The inset photographs in Figure 1f showed that the fluorescence emission color of SiNPs-C$_{18}$ remained blue, similar to that of SiNPs. The results shown in Figure 1f suggest the potential application of SiNPs-C$_{18}$ in bacterial imaging, more details of which will be reported below. Meanwhile, the fluorescence emission spectra of SiNPs-C$_{18}$ dissolved in different solvents with different polarities (including acetone, dichloromethane, ethanol, and water) were collected. In ethanol, SiNPs-C$_{18}$ generated the strongest fluorescence intensity, as a result of the best solubility of SiNPs-C$_{18}$ in ethanol (Figure 1f). This indicates that the fluorescence emission property of SiNPs-C$_{18}$ is influenced by the polarity of the solvent, which may imply that the fluorescence intensity of SiNPs-C$_{18}$ could be different when SiNPs-C$_{18}$ are present in water or in a less polar environment. We hope that such an intensity can significantly increase when SiNPs-C$_{18}$ are accumulated inside the bacterial cells, which will be discussed more below.

To further study the mechanism of the possible fluorescence signal intensity variation of SiNPs-C$_{18}$ in bacterial cells, we modeled Gram-positive bacterial cell membrane using liposomes composed of 1-palmitoyl-2-oleoyl-*sn*-glycero-3-phosphoethanolamine (POPE) and 1-palmitoyl-2-oleoyl-*sn*-glycero-3-phospho-(1'-*rac*-glycerol) (sodium salt) (POPG) (with a

molar ratio of POPE : POPG = 1 : 3)[28] prepared by a common vesicle extrusion method. The

resulting liposomes had an average diameter of 122.5 ± 1.9 nm, and a polydispersity index

of 0.133 measured by dynamic light scattering (DLS). After mixing varied concentrations of

liposomes with a fixed concentration of SiNPs-C$_{18}$ in phosphate buffer saline (PBS, pH = 7.4),

we found that the SiNPs-C$_{18}$ fluorescence intensity increased at elevated lipid

concentrations (from 0.1 to 2 mg/mL) (Figure 1g). A linear relationship between the

fluorescence intensity of SiNPs-C$_{18}$ and the liposome concentration was observed (Figure
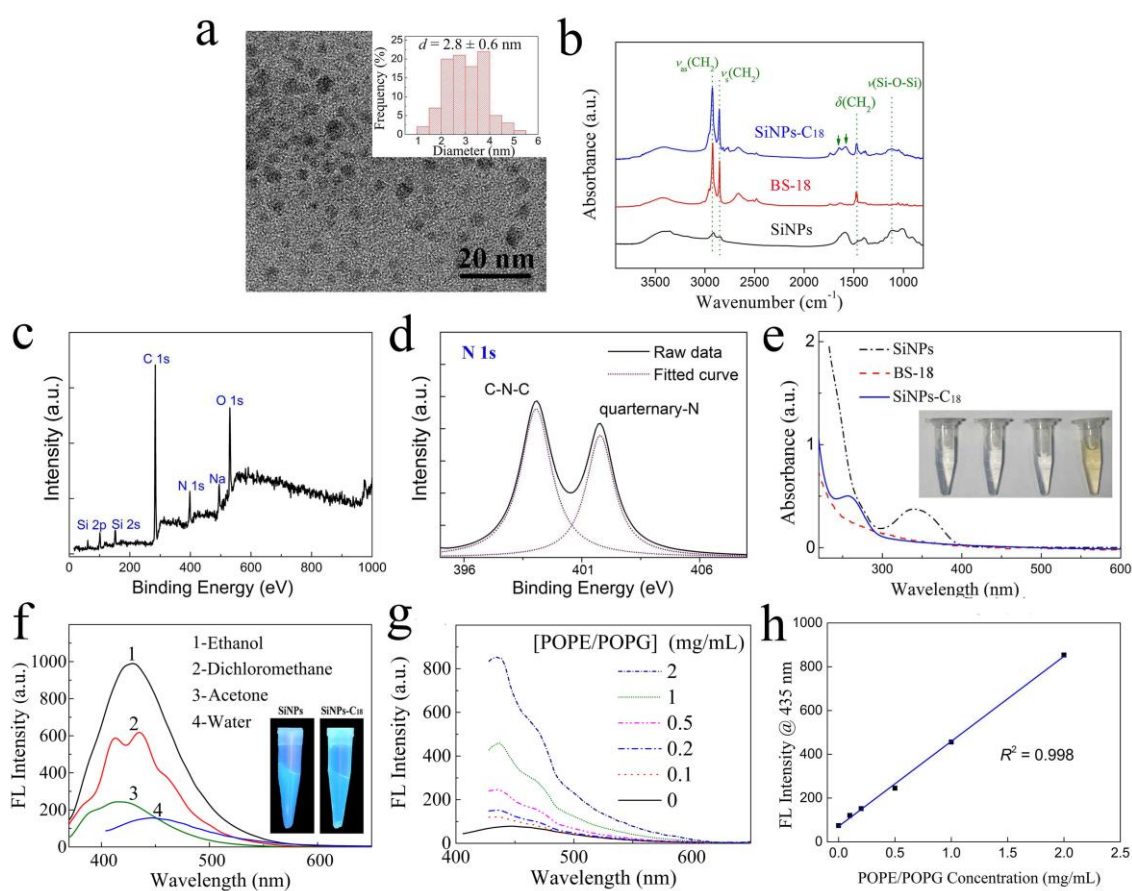
1h).

Figure 1. Characterizations of SiNPs-C$_{18}$. a) Typical TEM image and corresponding size distribution histogram (insert) of SiNPs-C$_{18}$. b) FTIR spectra of dried SiNPs-C$_{18}$, BS-18, and SiNPs. c) XPS spectrum of dried SiNPs-C$_{18}$ and d) the high resolution XPS peaks of N 1s. e) UV-vis absorption spectra of SiNP-C$_{18}$, BS-18, and SiNP aqueous solutions. The inset is the photograph of SiNPs-C$_{18}$ (100.0 μg/mL) in water, 0.9% NaCl, PBS, and LB medium, respectively (from left to right). f) Fluorescence spectra of SiNPs-C$_{18}$ dispersed in different solvents (including acetone, dichloromethane, ethanol, and water). The insets are photographs of SiNP and SiNP-C$_{18}$ aqueous solutions irradiated under a UV lamp (365 nm). g, h) Fluorescence responses of SiNPs-C$_{18}$ after mixing with POPE/POPG liposomes of different concentrations (0–2 mg/mL). The concentration of SiNPs-C$_{18}$ was fixed at 50 μg/mL.

2.2. Distinguishing Gram-positive and Gram-negative bacteria: Bacterial Imaging

In consideration of the excellent fluorescence property, we used the quaternized SiNPs for bacterial imaging. The imaging effect of the quaternized SiNPs (SiNPs-C_{18}) on various bacteria was tested. Our experiments showed that SiNPs-C_{18} could be used to selectively image the Gram-positive *S. aureus* bacteria, while the Gram-negative *E. coli* bacteria were rarely stained (**Figure 2**). Moreover, we also evaluated the staining effects of two other Gram-positive bacteria (*M. luteus* and *B. subtili*) and two other Gram-negative bacteria (*P. vulgaris* and *P. aeruginosa*). The results further confirmed the conclusion that SiNPs-C_{18} could specifically stain Gram-positive bacteria (**Figure S1**), making SiNPs-C_{18} useful to distinguish Gram-positive and Gram-negative bacteria using fluorescence imaging. This selective Gram-positive bacteria imaging effect can be explained by the strong interactions between SiNPs-C_{18} and cell walls/membranes of Gram-positive bacteria. The surface of Gram-positive bacteria, mainly containing negatively charged teichoic acids and a thick peptidoglycan layer, is easier to bind to quaternary ammonium compounds than that of Gram-negative ones composed of a lipopolysaccharide-linked outer membrane.[29] This caused the selective internalization of SiNPs-C_{18} into Gram-positive bacterial cells, which could not happen for the Gram-negative bacteria.
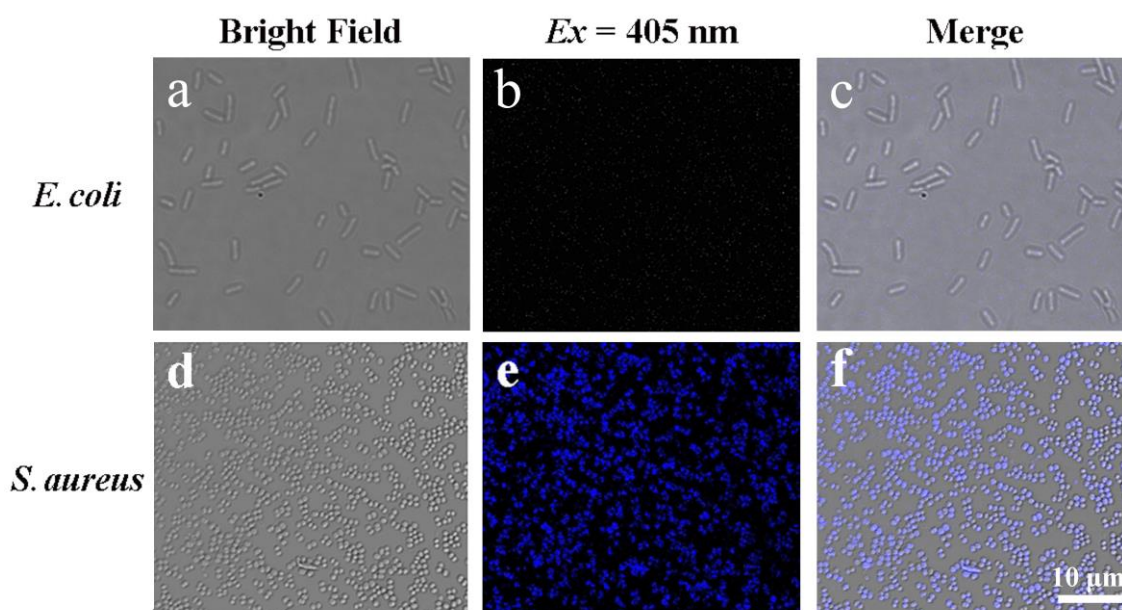
14

Figure 2. Confocal fluorescence images of a–c) *E. coli* and d–f) *S. aureus* bacteria after incubation with 0.5 µg/mL SiNPs-C$_{18}$ for 1 h and visualized under bright field, 405 nm excitation, and the overlay.

2.3. Antimicrobial Activity and Selectivity

2.3.1. In Vitro Antimicrobial Activity

As shown above, the quaternized SiNPs can differentiate Gram-positive bacteria from Gram-negative ones due to the different interactions between these SiNPs (e.g., SiNPs-C$_{18}$) and the two types of bacteria. Considering the widely used *N*-alkyl betaines for antibacterial application, we expect that the quaternized SiNPs can combine the antibacterial capability of *N*-alkyl betaines with the fluorescence property of SiNPs. A number of tests were performed to compare the antimicrobial effects of the SiNPs conjugated with a homologous

series of *N*-alkyl betaines (including BS-12, BS-14, BS-16, and BS-18). The antibacterial

activities of the quaternized SiNPs (SiNPs-C$_n$, n = 12, 14, 16, and 18) against *E. coli* and *S.*

aureus, which are representatives of Gram-negative and Gram-positive bacteria

respectively, were tested. All the quaternized SiNPs significantly decreased the viability of *S.*

aureus cells in a dose-dependent manner (**Figure 3**c). SiNPs-C$_{18}$ displayed the best

antibacterial effect, leading to the complete killing of *S. aureus* at a concentration of as low

as 1.0 μg/mL. While the SiNPs-C$_{16}$, SiNPs-C$_{14}$, and SiNPs-C$_{12}$ showed complete inactivation of

S. aureus bacteria at 5, 20, and 40 μg/mL respectively, indicating relatively weaker

antibacterial activities than SiNPs-C$_{18}$. To further demonstrate the best antibacterial effect

of SiNPs-C$_{18}$, all the MICs for *S. aureus* of the four quaternized SiNPs (SiNPs-C$_{12}$, SiNPs-C$_{14}$,

SiNPs-C$_{16}$, and SiNPs-C$_{18}$) were measured (**Table S1**). The results also revealed that a longer

hydrocarbon chain length of the betaine molecules on SiNPs led to a better antibacterial

activity against *S. aureus*. Differently, even at a high concentration of 40.0 μg/mL, all the

quaternized SiNPs could not inhibit the growth of Gram-negative *E. coli* effectively (Figure

3a).

To investigate the bacterial inhibitory and killing effects of SiNPs, free BS-18, and

SiNPs-C$_{18}$, the growth kinetics of *E. coli* and *S. aureus* in liquid media were studied (Figure 3b

and d). Bacterial growth was monitored by measuring the optical density at 600 nm (OD$_{600}$)

based on the turbidity of the cell suspension. The results showed that BS-18 could only

inhibit the growth of *S. aureus* within 10 h at a concentration of 10 μg/mL (Figure 3b). In

contrast, for SiNPs-C_{18} at the same concentration, the growth of the bacteria was completely

inhibited for at least 48 h. Different from the above results, no inhibition of the

Gram-negative *E. coli* bacteria was observed with BS-18 and SiNPs-C_{18} at 10 μg/mL. To

generalize our conclusion, we also measured the MICs of SiNPs-C_{18} against the other two

types of Gram-positive bacteria (*M. luteus* and *B. subtili*) and Gram-negative bacteria (*P.

vulgaris* and *P. aeruginosa*). The results further confirmed that SiNPs-C_{18} exhibited excellent

antibacterial activity only for Gram-positive bacteria (**Table 1**).

To observe the bacterial killing effect of SiNPs-C_{18} with naked eyes, the agar plate

experiments for *S. aureus* were also carried out (Figure 3e and f). Compared to the control

group, the SiNPs-treated group did not show noticeable difference in the number of

bacterial colonies, indicating that SiNPs could not inhibit the growth of *S. aureus*. Treatment

with BS-18 alone decreased the amount of bacteria to 70%, suggesting the incomplete

killing of bacteria with BS-18. In contrast, SiNPs-C_{18} could completely kill the bacteria,

showing the excellent antibacterial efficacy of SiNPs-C_{18} against *S. aureus*.

The antibacterial activities of free *N*-alkyl betaines were lower than those of quaternized

SiNPs (Figure 3, **Figure S2**, and Table S1). Two possible reasons contribute to the enhanced

antibacterial activity of the quaternized SiNPs compared with free *N*-alkyl betaines. First,

free *N*-alkyl betaines are electrically neutral since each of them contains a positively charged

quaternary ammonium group and a negatively charged carboxyl group. After conjugation

with SiNPs, the carboxyl group of betaine reacted with the amine group of SiNPs, resulting in the positively charged quaternized SiNPs (Scheme 1). Thus, the electrostatic interaction of the quaternized SiNPs with bacteria was stronger than that of free *N*-alkyl betaines. Second, because of the multi-valency effect of quaternized SiNPs, the local concentration of quaternary ammonium groups on the bacterial surface was higher than that for free *N*-alkyl betaines, enabling enhanced antibacterial activity of the quaternized SiNPs.
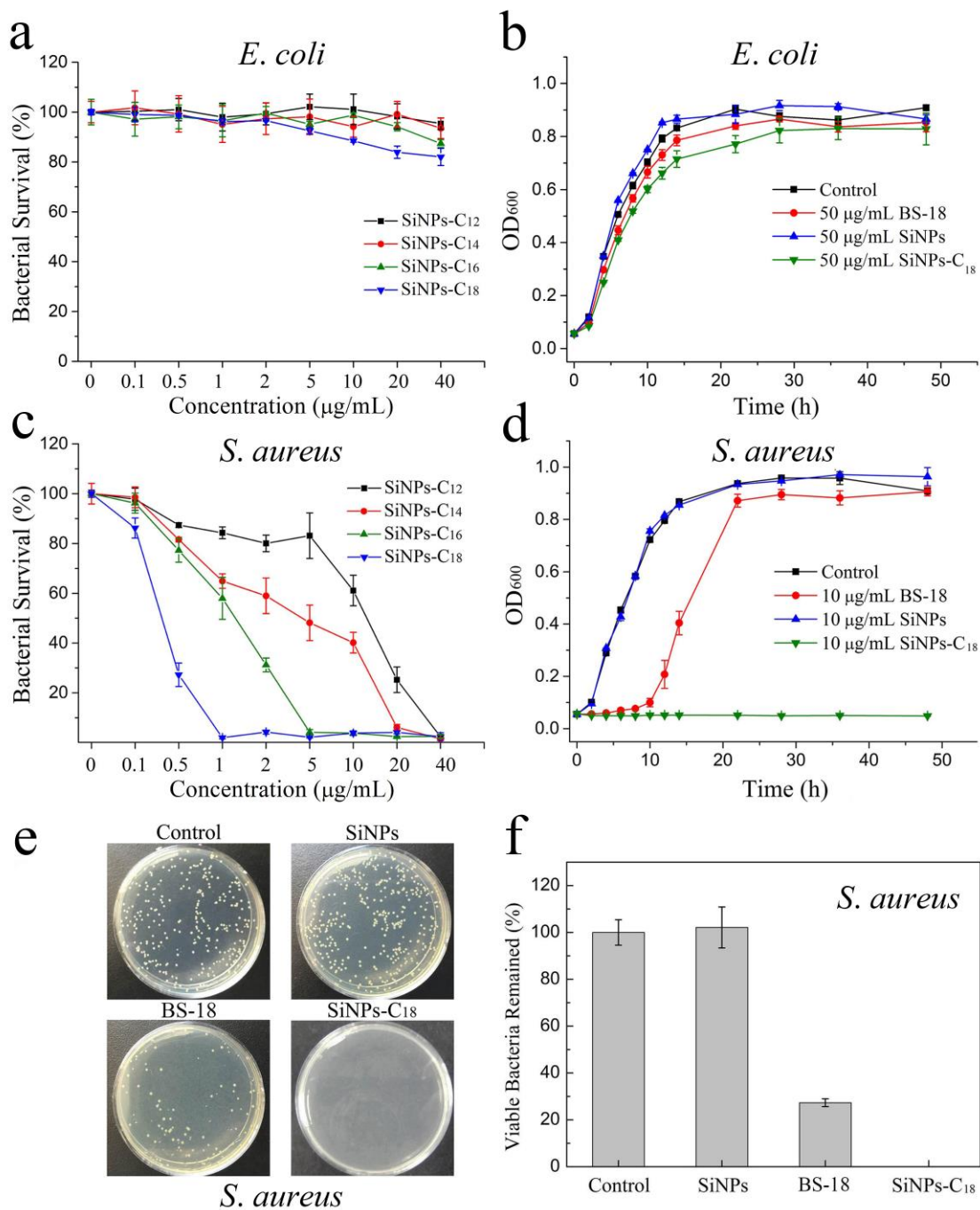
Figure 3. Concentration-dependent antimicrobial activities of SiNPs-C$_{12}$, SiNPs-C$_{14}$, SiNPs-C$_{16}$, and SiNPs-C$_{18}$ for a) *E. coli* and c) *S. aureus*. OD$_{600}$ of b) *E. coli* and d) *S. aureus* suspensions treated with BS-18, SiNPs, or SiNPs-C$_{18}$ measured at different times. e) Photographs of the

agar plates and f) corresponding statistical histograms of colonies of *S. aureus* after treatments with SiNPs, BS-18, or SiNPs-C$_{18}$.

Table 1. MICs of SiNPs-C$_{18}$ for three Gram-positive and three Gram-negative bacteria.

Species	Gram type	MIC (μg/mL)
S. aureus	G+	1
M. luteus	G+	1
B. subtili	G+	2
E. coli	G−	> 40
P. vulgaris	G−	> 40
P. aeruginosa	G−	> 40

2.3.2. Antimicrobial Mechanism

One major difference between Gram-positive and Gram-negative bacteria is that they have different cell wall/membrane structures. We therefore expect that SiNPs-C$_{18}$ can differentially kill Gram-positive or Gram-negative bacteria likely because they have different interactions between different bacteria cell walls/membranes, especially they can effectively damage/disrupt cell walls/membranes of Gram-positive bacteria.

Firstly we carried out scanning electron microscopic (SEM) experiments to test whether the integrity of bacterial cell walls can be disrupted by SiNPs-C$_{18}$. The SEM results showed that untreated *S. aureus* bacteria had globular morphology with smooth and intact cell walls (**Figure S3**c). After incubation with SiNPs-C$_{18}$ for 2 h, the cell walls of *S. aureus* became wrinkled and damaged, and the size and shape of the cells also changed dramatically. Moreover, for most of the bacterial cells, leakage of intracellular contents could be observed (Figure S3d). This confirmed that SiNPs-C$_{18}$ strongly interacted with Gram-positive bacterial cell walls and killed such bacteria by cell wall damaging/disruption. In contrast, no apparent morphological difference could be seen between treated and untreated *E. coli* cells (Figure S3a and b), indicating that SiNPs-C$_{18}$ did not disrupt the bacterial integrity and thus they exhibited negligible antibacterial effect.

To further investigate the antibacterial mechanism of SiNPs-C$_{18}$, Live/Dead staining assays using confocal imaging and flow cytometry were performed for *S. aureus* bacteria (**Figure 4**). SYTO 9 green-fluorescent nucleic acid dye is capable of labeling all bacteria with intact and damaged membranes.[30] In contrast, propidium iodide (PI) penetrates only bacteria with damaged membranes and binds nucleic acids with a concomitant enhancement of red fluorescence, causing a reduction in the fluorescence intensity of SYTO 9 dye when both dyes are present.[30] According to the confocal images presented in Figure 4a, the untreated and SiNP-treated bacteria showed only green fluorescence, with the red fluorescence percentage values quantified by flow cytometry as 0.3% and 1.4%, respectively (Figure 4b).

However, *S. aureus* treated with BS-18 and SiNPs-C$_{18}$ emitted much stronger red fluorescence, with the red fluorescence percentage values of 28.0% and 97.9%, respectively. The results indicated that SiNPs-C$_{18}$-treated *S. aureus* bacteria had completely disrupted cell walls/membranes, allowing the passage of PI dyes into the bacterial cells. In comparison, after incubation with SiNPs-C$_{18}$, *E. coli* emitted little red fluorescence (**Figure S4**). These results are well correlated to the SEM data discussed above.

In conclusion, the results from both SEM and Live/Dead staining assay experiments revealed that SiNPs-C$_{18}$ could damage the cell walls/membranes of *S. aureus*, change their permeability, and eventually lead to the death of *S. aureus*. The bacterial cell wall/membrane disruption ability enables SiNPs-C$_{18}$ to effectively combat bacterial drug resistance since it is difficult for bacteria to develop drug tolerance against membrane-disrupting antibiotics.[12f,31] We believe that SiNPs-C$_{18}$ can effectively disrupt the cell walls of Gram-positive bacteria through the following sequential events similar to quaternary ammonium compounds : (i) adsorb and insert into the cell wall through the strong electrostatic attraction with teichoic acids; (ii) interact with the cytoplasmic membrane (lipid or protein) followed by membrane damage; (iii) induce leakage of intracellular contents followed by bacterial death.[32] Since Gram-negative bacteria have different cell wall/membrane structures, SiNPs-C$_{18}$ could not destroy the cell walls/membranes of Gram-negative bacteria such as *E. coli*.
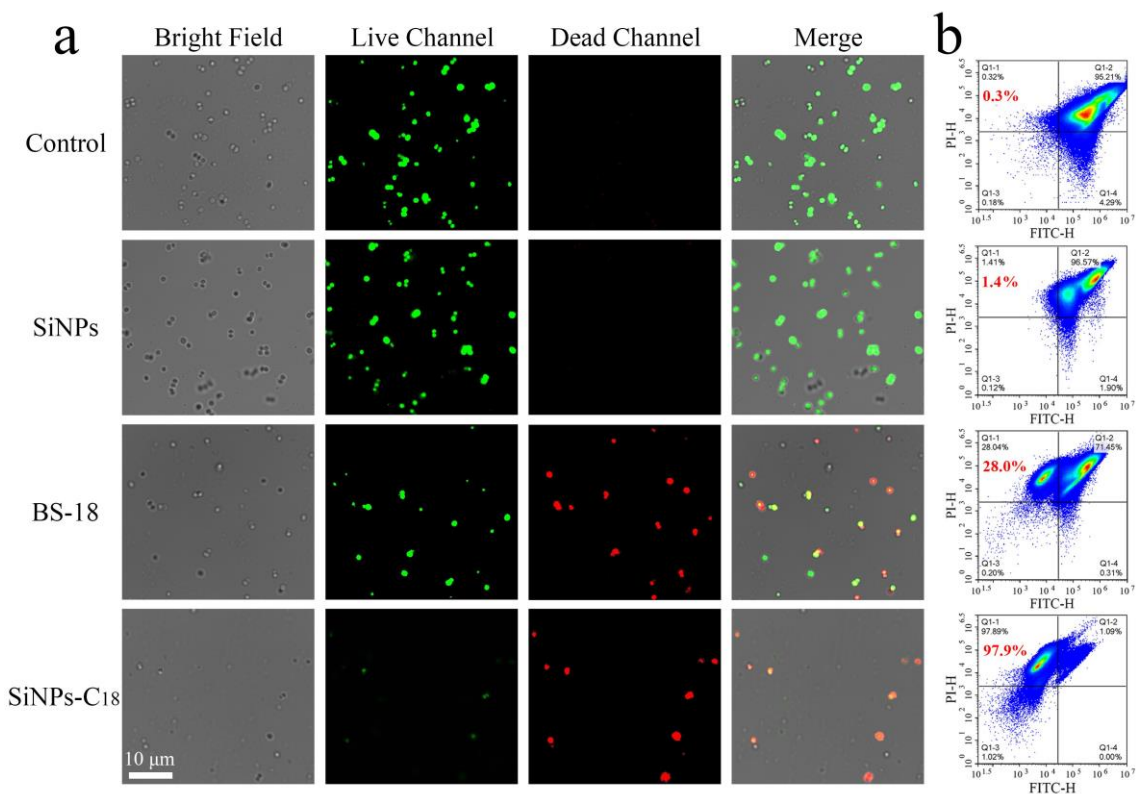
Figure 4. a) Confocal fluorescence images of *S. aureus* stained with BacLight Live/Dead kit showing the presence of live bacteria (green) and dead bacteria (red) in the LB solutions without the treatment (control) and with the treatments of 1 μg/mL SiNPs, BS-18, and SiNPs-C$_{18}$, and b) the corresponding analyses by flow cytometry.

2.3.3. Antibacterial Activity in S. aureus-Infected Macrophages

Mononuclear phagocyte system is one of the most important defense lines of the body to combat exogenous pathogens such as bacteria. Here we used bacteria-infected macrophages as a model system to examine the antibiotic activity of SiNPs-C$_{18}$ inside the macrophage cells to further demonstrate the feasibility of using SiNPs-C$_{18}$ for in vivo

application. The *S. aureus* bacteria were tagged with SYTO 9 dye before incubation with the macrophages (RAW 264.7 cells). Compared to the control and BS-18-treated groups, the amount of intracellular bacteria decreased significantly after adding SiNPs-C$_{18}$ (**Figure 5**a and b). The quantified fluorescence intensity using flow cytometry (Figure 5c) and the number of bacterial colonies in LB-agar plates (Figure 5d) further confirmed the strong antibiotic ability of SiNPs-C$_{18}$ toward *S. aureus* inside the macrophage cells. At the same time, the intact cell nuclei stained by the blue-fluorescent Hoechst 33343 dye in BS-18 and SiNPs-C$_{18}$ treated RAW 264.7 cells indicated that the cells were still alive. These experiments clearly showed that SiNPs-C$_{18}$ can effectively kill bacteria inside the macrophages (great antimicrobial activity) but do not kill macrophages (excellent selectivity).
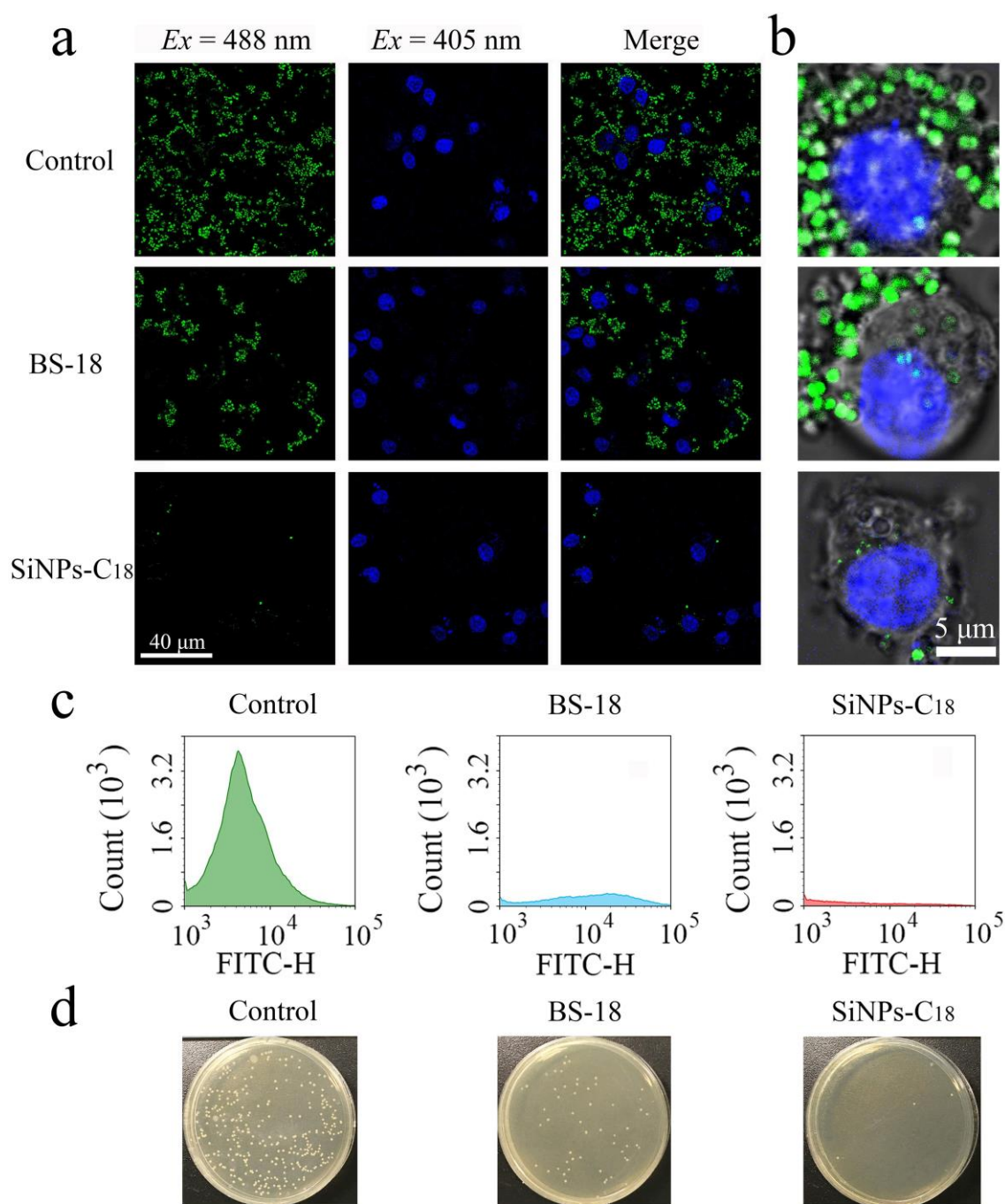
Figure 5. Examination of antibiotic activity in macrophages. a) Confocal fluorescence images of *S. aureus*-infected RAW 264.7 cells without (control) and with the treatments of BS-18 and SiNPs-C$_{18}$ for 2 h and b) the corresponding enlarged confocal fluorescence images. The *S. aureus* bacteria were tagged by green fluorescent SYTO 9 dye and the nuclei of RAW

264.7 cells were stained with blue-fluorescent Hoechst 33343 dye. c) Fluorescence intensity of intracellular *S. aureus* quantified by flow cytometry. d) Photographs of bacterial colonies formed on LB-agar plates.

2.3.4. In Vivo Antibacterial Activity

We also assessed the antibacterial efficacy of SiNPs-C$_{18}$ in vivo, utilizing *S. aureus*-infected mice as the model animals (**Figure 6**a). The mice were divided into two groups, including PBS-treated (control) and SiNPs-C$_{18}$-treated groups (Figure 6b). Therapeutic efficacy was evaluated by enumerating the bacterial counts in the LB-agar plates for the homogenized tissue dispersions from the infectious site (Figure 6c). After PBS treatment, quantification of the bacterial burden in the infectious tissue showed 3×10^6 CFU/g of *S. aureus* bacteria. Mice treated with SiNPs-C$_{18}$ showed a bacterial burden of 1.5×10^5 CFU/g, which was a significant reduction (with 95% bactericidal efficacy) compared to the PBS treated group.
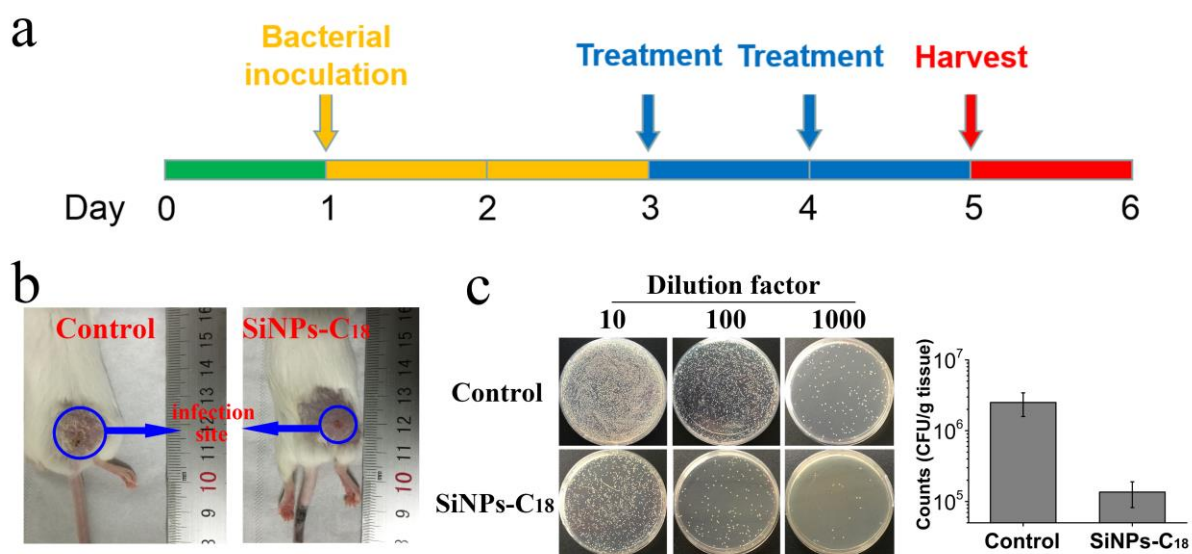
Figure 6. In vivo antibacterial test of SiNPs-C$_{18}$. a) The protocol of bacterium-infected model establishment, including bacterial inoculation and treatments before harvest. b) Photographs of *S. aureus*-infected mice treated with PBS (control) and SiNPs-C$_{18}$ after 2 d of bacterial infection. c) Photographs and the corresponding statistical histogram of bacterial colonies formed on the LB-agar plates derived from the homogenized tissue dispersions of the infected sites of mice injected with PBS and SiNPs-C$_{18}$, respectively. The tissue dispersions had been diluted (10, 100, and 1000 times) and plated on the LB-agar medium for 12 h at 37 ^{o}C before colony number counting.

2.4. In Vitro and In Vivo Safety Test

For any antimicrobial materials which are aimed for in vivo applications, it is necessary to ensure that they have excellent selectivity – That is, they should have great activity against bacteria but exhibit no toxicity towards mammalian cells. Here we evaluated the in vitro cytocompatibility of SiNPs-C$_{18}$ using MTT assays and AT II (normal lung cells) as well as L02

(normal liver cells) cells. SiNPs-C$_{18}$ showed no noticeable cytotoxicity to AT II or L02 cells at a concentration of up to 10.0 μg/mL (**Figure 7**a), which is much higher than the MICs for Gram-positive bacteria (Table 1). Meanwhile, hemolytic activity of SiNPs-C$_{18}$ was tested. Red blood cells in 0.1 M PBS and in 0.1% Triton X-100 solution were used for testing as negative control and positive control, respectively. Similar to the MTT results, no hemolytic activity was observed for SiNPs-C$_{18}$ at a concentration of up to 10.0 μg/mL (Figure 7b). In comparison, a significant hemolytic activity of BS-18 was observed at a low concentration of 2.0 μg/mL (**Figure S5**). The results indicate that SiNPs-C$_{18}$ have an excellent selectivity and meet the requirement to be used for in vivo applications, i.e., the applications in living systems, which will be reported below.

Finally, the in vivo toxicity of SiNPs-C$_{18}$ was also evaluated. The main organs of mice including heart, lung, liver, kidney, and spleen were collected and stained with hematoxylin and eosin (H&E). The tissues treated with SiNPs-C$_{18}$ maintained undisturbed structures (Figure 7c), demonstrating that the quaternized SiNPs are safe in vivo.
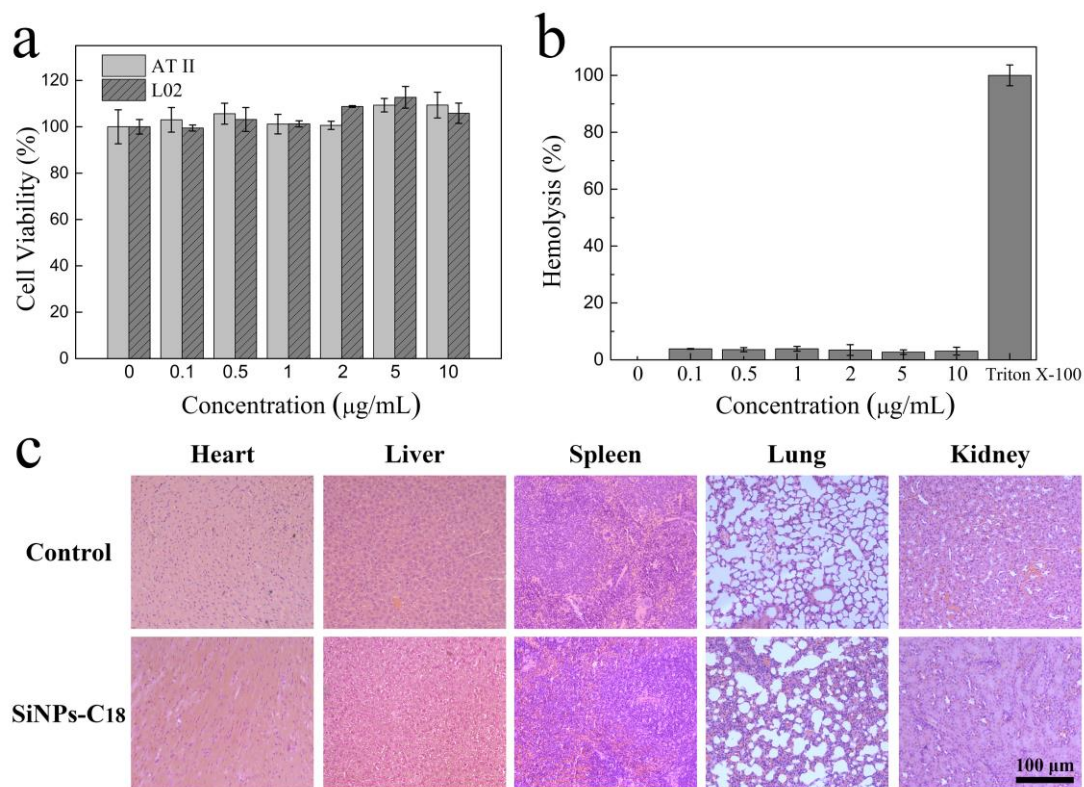
Figure 7. In vitro and in vivo safety evaluation. a) Cell viabilities of AT II and L02 cells treated with different dosages of SiNPs-C$_{18}$. b) Hemolysis results of different concentrations of SiNPs-C$_{18}$. Triton X-100 was set as the positive control. c) Histological evaluation of different organs (heart, liver, spleen, lung, and kidney) from mice treated with PBS and SiNPs-C$_{18}$.

2.5. Further Discussion.

Bacterial membranes have a significantly higher population of negative intrinsic curvature lipids than mammalian cell membranes,[33] which may account for the different killing effect of bacteria and mammalian cells by quaternized SiNPs. We believe the hydrophobic hydrocarbon chain and the positively charged surface endow these quaternized SiNPs with

excellent antibacterial property because they can effectively insert into the bacterial membranes through both hydrophobic and electrostatic interactions. Differently, they could not substantially interact with mammalian cell membranes, exhibiting excellent selectivity.

With the presence of both carboxyl and quaternary ammonium groups, the antibacterial effect of free *N*-alkyl betaines is limited due to their small net charge density. In contrast, by linking the *N*-alkyl betaines to the SiNPs, the negatively charged carboxyl groups are consumed and the resulting quaternized SiNPs possess a net charge of + 13.4 mV under physiological conditions. Furthermore, it has been reported that the isoelectric points (IEPs) of Gram-positive bacteria are generally lower than those of Gram-negative bacteria; therefore at a particular pH, Gram-positive bacteria are more negatively charged,[34] leading to the stronger interactions with quaternized SiNPs than Gram-negative bacteria. This resulted in the selective killing of Gram-positive bacteria by quaternized SiNPs. To sum up, compared to free *N*-alkyl betaines, the quaternized SiNPs have the following advantages: (a) more effective antibacterial activity of quaternized SiNPs for Gram-positive bacteria due to the multi-valency effect of NPs (Figure 3d-f and Table S1); (b) additional excellent fluorescence property to differentiate Gram-positive bacteria from Gram-negative ones (Figure 2 and Figure S1); (c) less cytotoxicity and better biocompatibility (Figure S5 and Figure 7).

When the quaternary ammonium salt-based antibacterial agents (such as the quaternized SiNPs) bind with the negatively charged surfaces of bacteria via electrostatic adsorption, the quaternary ammonium groups can replace Mg^{2+} and Ca^{2+},[35] the two main ions that can stabilize cell membranes, leading to the failure to vary the bacterial outer membrane permeability and the leakage of potassium ions and protons. Besides, quaternary ammonium derivatives with long hydrocarbon chains can penetrate through the cell wall and interact with the outer membrane of bacteria. The above two reasons may lead to the disruption of the bacterial outer membrane, leakage of bacterial cell content, and eventually the death of the bacteria. Because of the above antimicrobial activity mechanisms of SiNPs, it is difficult for bacteria to develop drug resistance.

After membrane association, the fluorescent quaternized SiNPs can accumulate within the less polar environment of Gram-positive bacteria, leading to highly fluorescent bacteria under laser irradiation. The simultaneous bacterial killing and imaging abilities of these quaternized SiNPs make them useful for bacterial detection and antimicrobial applications.

3. Conclusion

The present work provides the first example to prepare antibacterial SiNPs based on a simple one-step reaction between amine-containing fluorescent SiNPs and carboxyl-containing *N*-alkyl betaines. With many incomparable characteristics including

excellent water dispersibility and stability, superior optical properties, easy surface

modification capability, superb biocompatibility, and potential large-scale production ability,

the fluorescent SiNPs are being considered as ideal metal-free NPs for developing new

NP-based antibiotics. The as-prepared quaternized SiNPs exhibit polarity-dependent

fluorescence emission property and can simultaneously realize highly efficient killing and

imaging of Gram-positive bacteria, which can be explained by the synergistic electrostatic

and hydrophobic interactions between the more negatively charged Gram-positive bacteria

and the quaternized SiNPs. The low cytotoxicity and negligible hemolysis activity make

SiNPs-C$_{18}$ be potentially useful for in vivo antibacterial application. Moreover, the successful

application of SiNPs in selective bacterial imaging and killing develops a new research

direction of fluorescent metal-free nanodots (such as SiNPs and carbon dots). The

quaternized SiNPs have a promising prospect as alternatives to antibiotics, which will be

highly beneficial for human healthcare.

4. Experimental Section

Materials: (3-Aminopropyl)trimethoxysilane (APTMS), *N*,*N*-dimethyl-*N*-laurylbetaine (abbreviated

as BS-12) and *N*,*N*-dimethyl-*N*-myristylbetaine (abbreviated as BS-14) were purchased from Sigma

Aldrich. *N*,*N*-dimethyl-*N*-hexadecylbetaine (abbreviated as BS-16) and

N,*N*-dimethyl-*N*-octadecylbetaine (abbreviated as BS-18) were bought from Xinguang Chemical

Engineering Co. Ltd. (China). Sodium citrate dihydrate, *N*-hydroxysulfosuccinimide (NHS), and

N-(3-dimethylaminopropyl)-*N'*-ethylcarbodiimide hydrochloride (EDC) were obtained from Aladdin

(China). 1-palmitoyl-2-oleoyl-*sn*-glycero-3-phosphoethanolamine (POPE) and

1-palmitoyl-2-oleoyl-*sn*-glycero-3-phospho-(1'-*rac*-glycerol) (sodium salt) (POPG) were ordered from

Avanti Polar Lipids (USA). All the reagents were used without any further purification. All solutions

were prepared with deionized water (18.2 MΩ·cm) purified by a Milli-Q system (Millipore).

*Synthesis of SiNPs***:** The synthetic procedure of APTMS SiNPs has been reported previously. Briefly,

6.0 mL aqueous solution dissolved with 0.279 g trisodium citrate dihydrate in a 35.0 mL Ace pressure

tube was bubbled with nitrogen gas for 5 min. 1.5 mL of APTMS was then added into the above

solution under vigorous stirring. After filling the tube with nitrogen, the stirring was continued for

about 15 min to form SiNP precursors. The resultant precursor solution was then transferred into a

microwave reactor and processed under 160 $^{\circ}$C for 15 min, and cooled naturally to room

temperature. The residual reagents were removed by dialysis (1 kDa).

Synthesis of Quaternized SiNPs: BS-18 (120 mg) was dissolved in ethanol (1.0 mL) and mixed with

EDC/NHS in 0.1 M 2-(*N*-morpholino)ethanesulfonic acid (MES) buffer solution (pH = 6.0) at room

temperature. The molar ratio of BS-18 : NHS : EDC was 1 : 4 : 4. After 30 min, an SiNP (8 mg/mL)

phosphate buffered saline (PBS) solution (pH = 7.4, 5.0 mL) was added to the above solution and

reacted for another 12 h. The product was collected after dialysis (1 kDa) and freeze-drying.

SiNPs-C_{12}, SiNPs-C_{14}, and SiNPs-C_{16} were prepared in a similar method, just replacing BS-18 by BS-12, BS-14, and BS-16, respectively.

Characterization of SiNPs: Transmission electron microscopy (TEM) was carried out on a Tecnai G2 20 transmission electron microscope. The infrared spectra were collected with a Thermo Scientific Nicolet iS50 FT-IR spectrometer. Ultraviolet-visible (UV-vis) spectra were collected on a Shimadzu UV-2600 UV-vis spectrophotometer. X-ray photoelectron spectroscopy (XPS) analysis was conducted by a PHI Quantera II X-ray photoelectron spectrometer (Ulvac-Phi). Zeta potential measurements were carried out on a Malven Nano ZS Zetasizer. Fluorescence spectra were obtained using a Shimadzu RF-5301PC spectrofluorophotometer.

Preparation of Bacterial Model Membranes: POPE and POPG powders were weighed separately (with a molar ratio of 1 : 3) and dissolved in chloroform. The solvent was evaporated under nitrogen gas and the sample was further dried by vacuum overnight. The dried lipid film was rehydrated with PBS (0.1 M, pH = 7.4). The formed lipid suspension was vortexed for 30 s, sonicated in a bath sonicator for 1 min, and then extruded through a 100 nm pore-sized polycarbonate membrane for 21 times to form the final liposomes. For fluorescence measurements, the liposome solutions were diluted with PBS to twice the desired concentrations and mixed with an equal volume of 100 µg/mL SiNPs-C_{18} in PBS. The mixed solutions were stored at room temperature for 2 h before measurements.

Bacterial Culture: *Escherichia coli* (*E. coli*) and *Staphylococcus aureus* (*S. aureus*), used as the representative Gram-negative and Gram-positive bacteria, respectively, were cultured in lysogeny broth (LB) medium (5.0 mg/mL yeast extract, 10.0 mg/mL tryptone, and 0.5 mg/mL NaCl, pH = 7.0) on a shaking incubator (200 rpm) at 37 ^{o}C.

Bacterial Imaging Assay: 10 mL of bacteria suspension (1×10^5 to 1×10^6 CFU/mL) was treated with SiNPs-C$_{18}$ (0.5 µg/mL) for 2 h, collected by centrifugation at 5000 rpm for 5 min, and then imaged using a confocal microscope (TCS SP8, Leica, Germany).

Antibacterial Activity Measurement of Quaternized SiNPs: The bacteria solution incubated overnight was diluted 50 times for bacteria growth into log phase. The bacteria continued to grow for ~2 h until the optical density at 600 nm reached 0.5 (OD$_{600}$ = 0.5). Different quaternized SiNP solutions and the bacteria suspensions were added into the fresh LB broth to make the concentration of bacteria from 1×10^5 to 1×10^6 CFU/mL. After incubation for another 2 h, 100 µL of the suspension was dispersed in 96-well plates, followed by the addition of 10 µL CCK-8 solution to each well. The absorbance at 450 nm was measured by a Multiskan FC microplate photometer (Thermo).

LB-Agar Plates: 1.0 µg/mL SiNPs, BS-18, and SiNPs-C$_{18}$ solutions were added to *S. aureus* suspensions (1×10^5 to 1×10^6 CFU/mL), respectively. After treatment for 2 h, 100 µL of the diluted bacterial suspensions (1 : 1000 dilution) were then plated onto the agar plates. The number of bacterial colonies was counted after 24 h of incubation.

Real-Time Antibacterial Test: Bacteria suspensions (1×10^6 to 1×10^7 CFU/mL) treated with different materials were seeded in 96-well plates and cultured for more than 48 h on a shaking incubator (200 rpm) at 37 °C. During the culture process, the optical density at 600 nm of each well was monitored at different times.

Determination of MICs: Different concentrations of materials were added into the bacteria suspensions (1×10^5 to 1×10^6 CFU/mL) in a 96-well plate, and incubated for 18 h. The viability of the bacteria was measured by using the CCK-8 kit.

Morphological Characterization of Bacteria: Bacteria (1×10^5 to 1×10^6 CFU/mL) incubated with SiNPs-C$_{18}$ (1 μg/mL) for 2 h were collected by centrifugation at 5000 rpm for 10 min and fixed with 2.5% glutaraldehyde overnight at 4 °C. After washing with PBS for three times, the bacterial cells were dehydrated through sequential treatments of 30%, 50%, 70%, 80%, 90%, 95%, and 100% ethanol for 30 min and imaged using a scanning electron microscope (SEM, ULTRA Plus, Zeiss, Germany).

Live/Dead Staining: The LIVE/DEAD BacLight Bacterial Viability Kit provides a two-color fluorescence assay to test bacterial viability for a diverse array of bacteria. The Live/Dead staining experiments were carried out according to the manufacture's instructions. *S. aureus* cells (1×10^5 to 1×10^6 CFU/mL) treated with BS-18 and SiNPs-C$_{18}$ (1 μg/mL) for 2 h were collected by centrifugation at 8000 rpm for 5 min. After that, the bacteria were stained with green-fluorescent nucleic acid stain (SYTO 9) and red-fluorescent nucleic acid stain (propidium iodide, PI) for 30 min. The bacteria

samples were imaged using a confocal microscope (TCS SP8, Leica, Germany) and the fluorescence intensities were quantified using a flow cytometer (NovoCyte^{TM} 2060, ACEA, USA).

Examination of Antibiotic Activity in Macrophages: Bacterium-infected Raw 264.7 cells were prepared as model systems to examine the antibiotic activity of BS-18 and SiNPs-C$_{18}$ inside the macrophage cells. Firstly, bacteria were labeled with SYTO 9 green-fluorescent dye for bacteria visualization: SYTO 9 green-fluorescent dye was incubated with bacteria (~10^9 cells/mL) for 30 min, followed by centrifugation at 8000 rpm for 5 min. The supernatant was removed, and the precipitates were rinsed by normal saline solution for three times. Then the bacteria labeled with SYTO 9 were readily used for cellular uptake by macrophage cells.

Macrophages (RAW 264.7) (around 10^5 cells/mL) were incubated in DMEM medium at 37 °C. After incubation for 24 h, the cells were stained with Hoechst dye, which was prepared by mixing 0.5 μL Hoechst 33342 nuclear dye and 1.0 mL cell culture medium. The medium was then removed, and the remaining cells were rinsed with cell PBS solution twice. Next, the medium was replaced by fresh cell culture medium without antibiotics but containing green-fluorescent SYTO 9-labeled bacteria (around 10^7 CFU/mL), and the mixture was incubated for another 2 h at 37 ^{o}C. The medium was then removed, and the remaining cells were rinsed with cell PBS solution for four times. Subsequently, macrophages were incubated with DMEM medium containing 10 μg/mL SiNPs-C$_{18}$ for another 2 h after washing for four times with PBS. Furthermore, the infected macrophages treated with 10 μg/mL BS-18 were used as a control. The resultant cell samples were observed by a confocal

microscope (TCS SP8, Leica, Germany). The fluorescence intensities were quantified using a flow

cytometer (NovoCyte™ 2060, ACEA, USA).

To further quantify the antibacterial efficacy, 100 μL diluted bacterium-infected cell suspensions

without and with the treatment of SiNPs-C$_{18}$ (1 : 10 dilution) were then plated onto agar plates and

incubated at 37 °C. The number of bacterial colonies was counted after 18 h.

Mouse Infection Model: Four-week-old BALB/c female mice (25–30 g in weight) were purchased

from the Comparative Medicine Center of Yangzhou University (Jiangsu, China), and all animal

experimental procedures were performed according to the Guideline for Animal Experimentation

with the approval of the animal care committee of Southeast University. To evaluate the in vivo

antibacterial effect of SiNPs-C$_{18}$, the *S. aureus*-infected mouse model was built. 200 μL of *S. aureus* (1

× 10^9 CFU/mL) in PBS was subcutaneously injected into the mice. The mice were divided into two

groups, PBS- and SiNPs-C$_{18}$-treated groups. After 2-day infection, 200 μL of SiNPs-C$_{18}$ (1 mg/mL) in

PBS solution was injected into the infectious site once a day. All mice were sacrificed after treatment

for two days, and the infectious tissues and major organs (heart, liver, lung, kidney, and spleen) were

processed for further analyses. To determine the amount of the bacteria in the infectious tissues of

the mice, the infectious tissues were separated and homogenized in normal saline (1.0 mL). Aliquots

of diluted homogenized intestinal tissues were plated on LB agar, on which the grown colonies were

counted for analysis.

MTT Assay: To test the cytotoxicity of SiNPs-C$_{18}$ and BS-18, AT II cells (normal lung cells) and L02 (normal liver cells) were used in this study and were cultured in cell media (DMEM), supplemented with 10% fetal bovine serum, 100 U of penicillin, and 100 µg/mL streptomycin in a humidified incubator at 37 $^{\circ}$C and 5% CO$_2$. The cells (5 × 10^4 cells/well) were seeded in a 96-well plate in cell media overnight and then incubated with different concentrations of SiNPs-C$_{18}$ or BS-18 (0, 0.1, 0.5, 1, 2, 5, and 10 µg/mL) for 24 h. 10 µL MTT (5 mg/mL) was added to each well. After incubation for 4 h, 150 µL DMSO was added to each well. The absorbance at 492 nm was measured by a Multiskan FC microplate photometer (Thermo).

Hemolysis Assay: Healthy human blood (2 mL) was donated from a male volunteer. Red blood cells (RBCs) were collected by centrifugation at 3000 rpm for 10 min, washed with normal saline (0.9% NaCl) for three times, and resuspended using normal saline (100 mL) to prepare 2% erythrocyte solution. Then, different concentrations (0, 0.2, 1, 2, 4, 10, and 20 µg/mL) of SiNPs-C$_{18}$ or free BS-18 dissolved in normal saline solutions were added to the same-volume 2% erythrocyte solution in centrifuge tubes. After incubation at 37 $^{\circ}$C for 2 h, the supernatant was obtained through centrifugation at 2000 rpm for 10 min, and transferred to a 96-well plate. The absorbance at 450 nm was measured by a Multiskan FC microplate photometer (Thermo). RBCs in normal saline and in 1% Triton X-100 in normal saline were used as a negative control and a positive control, respectively. The following formula was used to calculate the hemolysis percentage:

Hemolysis (%) = (mean of absorbance value of treated group − mean of absorbance value of negative control group) / (mean of absorbance value of positive control − mean of absorbance value of negative control group) × 100%.

In Vivo Safety Test: Four-week-old BALB/c female mice were administered 200 μL of SiNPs-C$_{18}$ (1 mg/mL) once daily. Mice treated with PBS were tested in parallel as a negative control. After administration for two days, major organs were fixed in 4% formalin solution, processed routinely into paraffin and stained with haematoxylin and eosin (H&E). The pathologies were examined using an optical microscope.

Supporting Information

Supporting Information is available from the Wiley Online Library or from the author.

Acknowledgments

References and Notes

[1] a) N. Mendoza, P. Ravanfar, A. Satyaprakah, S. Pillai, R. Creed, *Dermatol. Ther.* **2009**, *22*, 129; b)
K. Vasilev, V. Sah, K. Anselme, C. Ndi, M. Mateescu, B. Dollmann, P. Martinek, H. Ys, L. Ploux, H.
J. Griesser, *Nano Lett.* **2010**, *10*, 202.

[2] a) Q. Bao, D. Zhang, P. Qi, *J. Colloid Interface Sci.* **2011**, *360*, 463; b) G. Sahni, P. Gopinath, P.
Jeevanandam, *Colloids Surf. B-Biointerfaces* **2013**, *103*, 441; c) S. B. Levy, B. Marshall, *Nat. Med.*
2004, *10*, S122.

[3] Y. Y. Zhao, C. J. Ye, W. W. Liu, R. Chen, X. J. Jiang, *Angew. Chem., Int. Ed.* **2014**, *53*, 8127.

[4] T. F. Tian, X. Z. Shi, L. Cheng, Y. C. Luo, Z. L. Dong, H. Gong, L. G. Xu, Z. T. Zhong, R. Peng, Z. Liu,
ACS Appl. Mater. Interfaces **2014**, *6*, 8542.

[5] X. N. Li, S. M. Robinson, A. Gupta, K. Saha, Z. W. Jiang, D. F. Moyano, A. Sahar, M. A. Riley, V. M.
Rotello, *ACS Nano* **2014**, *8*, 10682.

[6] Y. F. Zhou, X. X. Jiang, J. Tang, Y. Y. Su, F. Peng, Y. M. Lu, R. Peng, Y. He, *J. Mater. Chem. B* **2014**,
2, 691.

[7] a) M. E. Davis, Z. G. Chen, D. M. Shin, *Nat. Rev. Drug Discov.* **2008**, *7*, 771; b) R. Dastjerdi, M.
Montazer, *Colloids Surf. B-Biointerfaces* **2010**, *79*, 5; c) J. T. Seil, T. J. Webster, *Int. J.
Nanomedicine* **2012**, *7*, 2767.

[8] a) M. C. Daniel, D. Astruc, *Chem. Rev.* **2004**, *104*, 293; b) F. X. Redl, C. T. Black, G. C.
Papaefthymiou, R. L. Sandstrom, M. Yin, H. Zeng, C. B. Murray, S. P. O'Brien, *J. Am. Chem. Soc.*
2004, *126*, 14583.

[9] a) E. A. Azzopardi, E. L. Ferguson, D. W. Thomas, *J. Antimicrob. Chemother.* **2013**, *68*, 257; b) W.
L. Lee, W. C. Liles, *Curr. Opin. Hematol.* **2011**, *18*, 191; c) W. W. Gao, S. Thamphiwatana, P.
Angsantikul, L. F. Zhang, *Wiley Interdiscip Rev. Nanomed. Nanobiotechnol.* **2014**, *6*, 532.

[10] M. Liong, B. France, K. A. Bradley, J. I. Zink, *Adv. Mater.* **2009**, *21*, 1684.

[11] a) S. Loher, O. D. Schneider, T. Maienfisch, S. Bokorny, W. J. Stark, *Small* **2008**, *4*, 824; b) C. Marambio-Jones, E. M. V. Hoek, *J. Nanopart. Res.* **2010**, *12*, 1531; c) S. Chernousova, M. Epple, *Angew. Chem., Int. Ed.* **2013**, *52*, 1636; d) A. Alonso, X. Muñoz-Berbel, N. Vigués, R. Rodríguez-Rodríguez, J. Macanás, M. Muñoz, J. Mas, D. N. Muraviev, *Adv. Funct. Mater.* **2013**, *23*, 2450; e) X. N. Hu, Y. Y. Zhao, Z. J. Hu, A. Saran, S. Hou, T. Wen, W. Q. Liu, Y. L. Ji, X. Y. Jiang, X. C. Wu, *Nano Res.* **2013**, *6*, 822; f) Y. Tian, J. J. Qi, W. Zhang, Q. Cai, X. Y. Jiang, *ACS Appl. Mater. Interfaces* **2014**, *6*, 12038; g) O. Akhavan, E. Ghaderi, *Sci. Technol. Adv. Mater.* **2016**, *10*, 015003; h) M. Hoop, Y. Shen, X. Z. Chen, F. Mushtaq, L. M. Iuliano, M. S. Sakar, A. Petruska, M. J. Loessner, B. J. Nelson, S. Pané, *Adv. Funct. Mater.* **2016**, *26*, 1063.

[12] a) G. Ren, D. Hu, E. W. Cheng, M. A. Vargas-Reus, P. Reip, R. P. Allaker, *Int. J. Antimicrob. Agents* **2009**, *33*, 587; b) Y. Y. Zhao, Y. Tian, Y. Cui, W. W. Liu, W. S. Ma, X. Y. Jiang, *J. Am. Chem. Soc.* **2010**, *132*, 12349; c) Y. Y. Zhao, X. Y. Jiang, *Nanoscale* **2013**, *5*, 8340; d) C. Kaweeteerawat, C. H. Chang, K. R. Roy, R. Liu, R. B. Li, D. Toso, H. Fischer, A. Ivask, Z. X. Ji, J. I. Zink, *ACS Nano* **2015**, *9*, 7215; e) S. H. Cha, J. Hong, M. McGuffie, B. Yeom, J. S. VanEpps, N. A. Kotov, *ACS Nano* **2015**, *9*, 9097; f) H. Y. Wang, X. W. Hua, F. G. Wu, B. L. Li, P. D. Liu, N. Gu, Z. F. Wang, Z. Chen, *ACS Appl. Mater. Interfaces* **2015**, *7*, 7082; g) G. Applerot, A. Lipovsky, R. Dror, N. Perkas, Y. Nitzan, R. Lubart, A. Gedanken, *Adv. Funct. Mater.* **2009**, *19*, 842.

[13] a) W. B. Hu, C. Peng, W. J. Luo, M. Lv, X. M. Li, D. Li, Q. Huang, C. H. Fan, *ACS Nano* **2010**, *4*, 4317; b) J. M. Zhao, B. Deng, M. Lv, J. Y. Li, Y. J. Zhang, H. Q. Jiang, C. Peng, J. Li, J. Y. Shi, Q. Huang, C. H. Fan, *Adv. Healthc. Mater.* **2013**, *2*, 1259; c) F. Perreault, A. F. de Faria, S. Nejati, M. Elimelech, *ACS Nano* **2015**, *9*, 7226; d) X. Zou, L. Zhang, Z. Wang, Y. Luo, *J. Am. Chem. Soc.* **2016**, *138*, 2064.

[14] A. J. Friedman, J. Phan, D. O. Schairer, J. Champer, M. Qin, A. Pirouz, K. Blecher-Paz, A. Oren, P. T. Liu, R. L. Modlin, J. Kim, *J. Invest. Dermatol.* **2013**, *133*, 1231.

[15] a) Z. Drulis-Kawa, A. Dorotkiewicz-Jach, *Int. J. Pharm.* **2010**, *387*, 187; b) D. Pornpattananangkul, V. Fu, S. Thamphiwatana, L. Zhang, M. Chen, J. Vecchio, W. W. Gao, C. M. Huang, L. F. Zhang, *Adv. Healthc. Mater.* **2013**, *2*, 1322; c) S. Thamphiwatana, W. W. Gao, M. Obonyo, L. F. Zhang, *Proc. Natl. Acad. Sci. U.S.A.* **2014**, *111*, 17600.

[16] a) L. H. Liu, K. J. Xu, H. Y. Wang, P. K. Tan, W. M. Fan, S. S. Venkatraman, L. J. Li, Y. Y. Yang, *Nat. Nanotechnol.* **2009**, *4*, 457; b) Z. Y. Ong, N. Wiradharma, Y. Y. Yang, *Adv. Drug Deliv. Rev.* **2014**, *78*, 28.

[17] E. Ryu, *J. Jpn. Soc. Vet. Sci.* **1938**, *17*, 31.

[18] R. K. Sizemore, J. J. Caldwell, A. S. Kendrick, *Appl. Environ. Microb.* **1990**, *56*, 2245.

[19] E. Rojas, J. A. Theriot, K. C. Huang, *Proc. Natl. Acad. Sci. U.S.A.* **2014**, *111*, 7807.

[20] a) H. J. Chung, T. Reiner, G. Budin, C. Min, M. Liong, D. Issadore, H. Lee, R. Weissleder, *ACS Nano* **2011**, *5*, 8834; b) D. Zhong, Y. Zhuo, Y. J. Feng, X. M. Yang, *Biosens. Bioelectron.* **2015**, *74*, 546.

[21] a) J. H. Warner, A. Hoshino, K. Yamamoto, R. Tilley, *Angew. Chem., Int. Ed.* **2005**, *44*, 4550; b) N. O'Farrell, A. Houlton, B. R. Horrocks, *Int. J. Nanomed.* **2006**, *1*, 451; c) F. Erogbogbo, K. T. Yong, I. Roy, G. Xu, P. N. Prasad, M. T. Swihart, *ACS Nano* **2008**, *2*, 873; d) N. H. Alsharif, C. E. Berger, S. S. Varanasi, Y. Chao, B. R. Horrocks, H. K. Datta, *Small* **2009**, *5*, 221; e) Y. He, Z. H. Kang, Q. S. Li, C. H. A. Tsang, C. H. Fan, S. T. Lee, *Angew. Chem., Int. Ed.* **2009**, *48*, 128; f) S. Chinnathambi, S. Chen, S. Ganesan, N. Hanagata, *Adv. Healthc. Mater.* **2014**, *3*, 10; g) F. Peng, Y. Y. Su, Y. L. Zhong, C. H. Fan, S. T. Lee, Y. He, *Acc. Chem. Res.* **2014**, *47*, 612.

[22] a) M. Dasog, Z. Y. Yang, S. Regli, T. M. Atkins, A. Faramus, M. P. Singh, E. Muthuswamy, S. M. Kauzlarich, R. D. Tilley, J. G. Veinot, *ACS Nano* **2013**, *7*, 2676; b) X. T. Lu, C. M. Hessel, Y. X. Yu, T. D. Bogart, B. A. Korgel, *Nano Lett.* **2013**, *13*, 3101; c) F. Priolo, T. Gregorkiewicz, M. Galli, T. F. Krauss, *Nat. Nanotechnol.* **2014**, *9*, 19.

[23] Y. X. Zhang, X. Han, J. M. Zhang, Y. Liu, H. Huang, H. Ming, S. T. Lee, Z. H. Kang, *Nanoscale* **2012**, *4*, 7760.

[24] Z. H. Kang, C. H. A. Tsang, N. B. Wong, Z. D. Zhang, S. T. Lee, *J. Am. Chem. Soc.* **2007**, *129*, 12090.

[25] a) X. D. Zhang, X. K. Chen, S. Q. Kai, H. Y. Wang, J. J. Yang, F. G. Wu, Z. Chen, *Anal. Chem.* **2015**, *87*, 3360; b) X. Y. Ji, F. Peng, Y. L. Zhong, Y. Y. Su, X. X. Jiang, C. X. Song, L. Yang, B. B. Chu, S. T. Lee, Y. He, *Adv. Mater.* **2015**, *27*, 1029; c) R. D. Tilley, K. Yamamoto, *Adv. Mater.* **2006**, *18*, 2053.

[26] F. G. Wu, X. D. Zhang, S. Q. Kai, M. Y. Zhang, H. Y. Wang, J. N. Myers, Y. X. Weng, P. D. Liu, N. Gu, Z. Chen, *Adv. Mater. Interfaces* **2015**, *2*, 1500360.

[27] a) C. S. Yang, R. A. Bley, S. M. Kauzlarich, H. W. Lee, G. R. Delgado, *J. Am. Chem. Soc.* **1999**, *121*, 5191; b) M. Rosso-Vasic, E. Spruijt, B. van Lagen, L. De Cola, H. Zuilhof, *Small* **2008**, *4*, 1835.

[28] J. Lee, S. W. Jung, A. E. Cho, *Langmuir* **2016**, *32*, 1782.

[29] a) H. X. Yuan, Z. Liu, L. B. Liu, F. Lv, Y. L. Wang, S. Wang, *Adv. Mater.* **2014**, *26*, 4333; b) H. Y. Wang, X. W. Hua, H. R. Jia, C. C. Li, F. M. Lin, Z. Chen, F. G. Wu, *ACS Biomater*. *Sci*. *Eng*. **2016**, DOI: 10.1021/acsbiomaterials.6b00130; c) O. Wiarachai, N. Thongchul, S. Kiatkamjornwong, V. P. Hoven, *Colloids Surf. B-Biointerfaces* **2012**, *92*, 121.

[30] L. Boulos, M. Prevost, B. Barbeau, J. Coallier, R. Desjardins, *J. Microbiol. Methods* **1999**, *37*, 77.

[31] H. Chen, B. Wang, J. Y. Zhang, C. Y. Nie, F. T. Lv, L. B. Liu, S. Wang, *Chem. Commun.* **2015**, *51*, 4036.

[32] G. McDonnell, A. D. Russell, *Clin. Microbiol. Rev.* **1999**, *12*, 147.

[33] a) L. Yang, V. D. Gordon, A. Mishra, A. Som, K. R. Purdy, M. A. Davis, G. N. Tew, G. C. Wong, *J. Am. Chem. Soc.* **2007**, *129*, 12141; b) A. Som, L. H. Yang, G. C. Wong, G. N. Tew, *J. Am. Chem. Soc.* **2009**, *131*, 15102.

[34] J. W. Bartholomew, T. Mittwer, *Bacteriol. Rev.* **1952**, *16*, 1.

[35] a) M. Vaara, *Microbiol. Rev.* **1992**, *56*, 395; b) J. Yatvin, J. Gao, J. Locklin, *Chem. Commun.* **2014**, *50*, 9433; c) Y. Xue, H. N. Xiao, Y. Zhang, *Int. J. Mol. Sci.* **2015**, *16*, 3626.

TOC Graphic
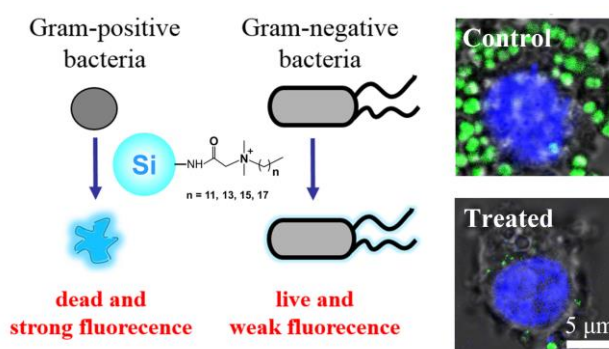
A simple and efficient method was developed based on fluorescent quaternized silicon nanoparticles (SiNPs) to meet the increasing demands of bacterial differentiation and metal-free NP-based antibiotics. The quaternized SiNPs with polarity-dependent fluorescence emission possessed superb selectivity to image and kill Gram-positive bacteria over Gram-negative ones. The low cytotoxicity of quaternized SiNPs enables them for future clinical application.